J Mater Sci (2010) 45:2780–2787
DOI 10.1007/s10853-010-4267-0

Response of radiation dosimeters based on in situ oxygen plasma post-treated CVD-diamond thin films to X-ray

Xiaoming Liao · Junguo Ran · Li Gou

Received: 8 October 2009 / Accepted: 26 January 2010 / Published online: 9 February 2010
© Springer Science+Business Media, LLC 2010

Abstract Radiation dosimeters based on in situ oxygen plasma post-treated diamond thin films were fabricated in a simple sandwich configuration. Effects of deposition process, methane concentration, and in situ oxygen plasma post-treatment on the sensitivity of the devices to X-ray irradiation were investigated. X-ray response demonstrates that the cyclic deposition process could improve response sensitivity. The increase in methane concentration in the deposition gas mixture will worsen the irradiation response of the devices mainly resulted from the change of the orientation and purity of the films. X-ray photoelectron spectroscopy, photoluminescence, and Raman measurements suggest that in situ oxygen plasma post-treatment can effectively etch non-diamond phases and passivate the silicon-vacancy and nitrogen-vacancy defects of the diamond films, resulting in an increase in the sensitivity of the device by a factor of about 2. Time-dependent response to X-ray indicates that the extended period to achieve photocurrent signals stability for the devices is a limitation for promising applications in radiation dosimetry.

Introduction

Diamond has a number of properties that make it a potentially remarkable material for use as a radiation dosimeter including efficient room temperature operation, chemical inertness, high-temperature operation stability, high radiation hardness, the resistance to high irradiation fluxes, and its tissue equivalence [1–6], which indicates that there is no need to apply energy-dependent signal corrections as a radiation dosimeter. Published works on natural diamond dosimeters [7–9] indicate that they may be suitable for both photon and electron dosimetries over a wide rang of energies without the need for selective energy compensation as is required for silicon dosimeters, and have higher sensitivity and spatial resolution than Si diodes. However, the difficulty in selecting suitable natural diamond has limited their application.

Advances in the synthesis of diamond by chemical vapor deposition (CVD) technology, which allows diamond films to deposit in a controllable and reproducible way, have resulted in an improvement in the quality and availability of material suitable for radiotherapy dosimetry [9, 10]. Unfortunately, CVD diamond prepared by current methods is generally a polycrystalline material, which is usually characterized by the presence of high concentration of bulk defects [11]. Especially, the presence of deep levels (defect-related trapping) in the gap may give rise to priming effects which can influence the measurement during radiation [12–17]. In general, the performance of the CVD diamond is correlated to the diamond quality, which, in turn, is heavily influenced by the deposition and post-treatment conditions. So, the improvement in the quality of the diamond thin films has been a highlight to optimize the dosimetric properties of the CVD diamond-based device. In this article, the quality of the microwave plasma chemical vapor deposition (MWPCVD) diamond thin films was improved using the cyclic deposition process and in situ oxygen plasma post-treatment. The effects of different deposition processes, methane concentration, and in situ oxygen plasma post-treatment on the X-ray response performance of the diamond films were investigated. The priming behavior of the MWPCVD diamond thin film was also involved.

X. Liao (✉) · J. Ran · L. Gou
College of Materials Science and Engineering, Sichuan University, Chengdu 610064, People's Republic of China
e-mail: sherman_xm@163.com

Experimental

Diamond thin films were deposited on (100) p-type Si substrates purchased from Emei Semiconductor Materials Plant (Emei City, China), which were polished with diamond powders to promote nucleation, by a bell jar-type MWPCVD deposition technique equipped with 2.45 GHz microwave generator. All the diamond thin films were deposited with the following nucleation conditions: the microwave power of 1.3 kW, pressure of 5.3 kPa, substrate temperature of 960 °C, CH_4 concentration of 1.08% in hydrogen, and nucleation time of 1 h. The growth conditions are the same as the nucleation conditions except that the microwave power was 1.2 kW, and that CH_4 concentration was varied from 0.34 to 0.60%. The deposition time and the film thickness of all the studied samples are 12 h and about 4 μm, respectively. RD1 and RD2 were prepared from hydrogen–methane precursor mixture of 0.34% methane by the nucleation-growth deposition process and the nucleation-etching-growth deposition process, respectively. The main difference of the above two deposition processes is that the latter will temporarily close methane gas for 30 min after the nucleation step so as to let hydrogen etch non-diamond phase formed in the nucleation period under the microwave power of 1 kW. With the cyclic deposition process, which refers to the intermittent close of methane gas after every 1 h growth so as to let hydrogen etch non-diamond phase formed in the growth period for 20 min, RD3, RD4, RD5, and RD6 were synthesized under the CH_4 gas concentration 0.34, 0.43, 0.51, and 0.60%, respectively. In order to minimize surface leakage currents, based on our previous study [18], in situ oxygen plasma post-treatment was employed for all the above as-grown diamond thin films with the microwave power of 400 W, oxygen flow rate of 30 mL/min, pressure of 2.6 kPa, and post-treatment time of 20 min. The substrate temperature was measured using IR pyrometer (SCJ-2MK, China). The relative content of surface carbon combined states of the in situ plasma post-treated diamond film was characterized and analyzed through X-ray photoelectron spectroscopy (XPS, Kratos XSAM800, England) with a hemispherical energy analyzer and using a monochromatic Al Kα source (1486.6 eV). As the delay-line detector allows a high count rate, the power applied to the X-ray anode was 144 W in order to minimize the possible X-ray-induced degradation of the samples. The instrument work function was calibrated to give a binding energy of 83.96 eV for the Au 4f7/2 line for metallic gold and the spectrometer dispersion was adjusted to give a binding energy of 932.62 eV for Cu 2p2/3 line for metallic copper. The Raman spectra were recorded in the range 1000–2000 cm^{-1} using a JY-HR800 spectrometer (JY-HR800, Jobin-Yvon, France) with an Ar^+ laser (532 nm line) as the excitation source. The structure and the surface morphology of the samples were characterized by X-ray diffraction (XRD, Philips X'Pert Pro, the Netherlands) using Cu Kα radiation as the source and scanning electron microscopy (SEM, JSM-5900, Japan), respectively. The photoluminescence (PL) measurements were performed at room temperature on the Fluorescence Spectrophotometer (F-7000, Hitachi, Japan) using a Xe laser as the excitation light source and with the excitation wavelength 420 nm. RD7 refers to the as-grown film prepared with the same conditions as the RD3, whereas RD3 was additionally post-treated with in situ oxygen plasma.

In our study, all the radiation dosimeters were fabricated in a simple sandwich structure (Pt/diamond thin film/silicon). Pt was sputtered on the growth side of the diamond films as the front contact with the size of 81 mm^2 × 600 nm. The Si substrate was used as the back electrode contact. In order to obtain better ohmic contacts, all the devices were then annealed in argon atmosphere at 450 °C for 30 min. The resistivities of the samples were obtained from the dark current measurements by the ZC36 10^{-14} A Measure Unit. Photocurrents under steady-state X-ray irradiation from Philips X'pert Pro diffractometer were also measured by the ZC36 10^{-14} A Measure Unit with an applied voltage of 5 V. In addition, to test X-ray radiation response of the diamond dosimeters under various X-ray fluxes, aluminum foils with different thickness were used to attenuate the direct beam so as to conveniently adjust the X-ray intensity. The deposition process, resistivities, and sensitivities of all the investigated samples were listed in Table 1.

Results and discussion

Effect of deposition process

From Table 1, it can be seen that the resistivities of RD1, RD2, and RD3 were 1.1 × 10^{12}, 2.5 × 10^{13}, and 6.8 × 10^{14} Ω cm, respectively, showing that the cyclic deposition technique can increase the resistivity about more than two orders of magnitude compared with the nucleation-growth process. This is because activated hydrogen etches graphite at a much higher rate than it does diamond [19, 20], and hydrogen ion treatment can effectively eliminate the impurities between the grain boundaries to improve the film purity. Figure 1 shows the photocurrents at different X-ray fluxes for radiation dosimeters based on diamond thin films prepared by different deposition procedures, showing that the response of the devices is linear with X-ray flux. This suggests that through correction the dosimeter based on the thin film could be used in radiation dosimetry.

Table 1 Deposition process, resistivity, and sensitivity of the different samples

Sample ID	Nucleation	H-etch	Growth		Post O-plasma	Resistivity (Ω cm)	Sensitivity (photocurrent slope)
			CH_4 content (vol.%)	Periodic H-etch			
RD1	√	×	0.34	×	√	1.1×10^{12}	9.13×10^{-5}
RD2	√	√	0.34	×	√	2.5×10^{13}	1.08×10^{-4}
RD3	√	√	0.34	√	√	6.8×10^{14}	1.45×10^{-4}
RD4	√	√	0.43	√	√	4.5×10^{14}	1.13×10^{-4}
RD5	√	√	0.51	√	√	3.2×10^{14}	9.50×10^{-5}
RD6	√	√	0.60	√	√	1.2×10^{14}	6.85×10^{-5}
RD7	√	√	0.34	√	×	5.9×10^{11}	7.83×10^{-5}

"√" means that this step was employed in the deposition process of the sample, while "×" means not

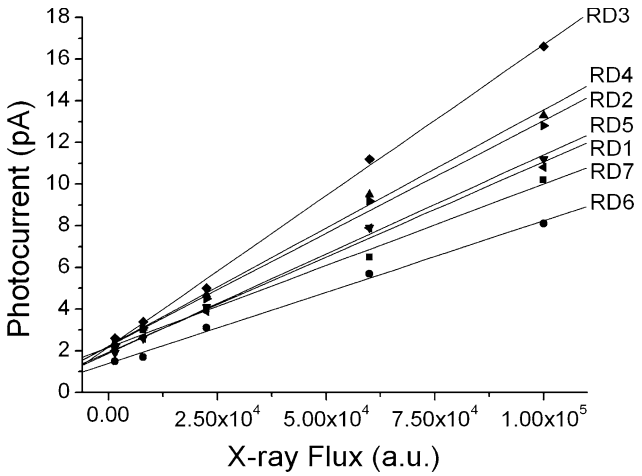

Fig. 1 Photocurrents versus X-ray flux curves of the radiation dosimeters based on the different samples

In this article, the sensitivity of the devices to X-ray irradiation is defined by the ratio of the photocurrent to X-ray flux of the incident radiation, i.e., the slope of the photocurrent as a function of the X-ray flux. Figure 1 shows that the slopes of the curves for the obtained samples are different. RD3 has the highest slope in comparison with the other samples, indicating that RD3 has the highest sensitivity. Table 1 shows that RD3 has the highest sensitivity (1.45×10^{-4}) compared with RD2 (1.08×10^{-4}) and RD1 (9.13×10^{-5}). The difference among them is mainly resulted from the different purities of the films, which is in accordance with the resistivities of the samples from the dark current measurements. The results also suggest that the cyclic deposition technique may be an effective means to improve the photoelectric performance of CVD diamond-based devices.

Effect of methane concentration

The typical SEM images of sample RD1 prepared by nucleation-growth technique and the oriented diamond films prepared under different methane concentrations using cyclic deposition technique were shown in Fig. 2. The film surface shown in Fig. 2(a) [RD3], (b) [RD4], (c) [RD5], and (e) [RD1] is composed of cubic (100) growth facets corresponding to [100]-orientation, whereas the film surface shown in Fig. 2d [RD6] is composed of triangular (111) growth facets corresponding to [111]-orientation. Figure 2 shows also that the sample RD3 has more well-defined cubic (100) growth facets than the samples RD4, RD1, and RD5, respectively. Compared with sample RD3, sample RD1 prepared by nucleation-growth technique exhibits some cauliflower-like structure mainly resulted from the secondary nucleation and the deterioration of quality of diamond films. Figure 3 shows the XRD patterns of the diamond films. It could be seen that only four peaks corresponding to the (111), (220), (311), and (400) were detected. No characteristic peaks of crystalline graphite were observed. The intensity ratios of $I_{(100)}/I_{(111)}$ for the samples RD3, RD4, RD5, and RD1 calculated from Fig. 3 were 1.02, 0.96, 0.49, and 0.89, respectively, larger than that of natural diamond (0.07), indicating a very strong [100]-orientation. But for RD6 the intensity ratio of $I_{(100)}/I_{(111)}$ was 0.06, showing a strong [111]-orientation. The decrease in the intensity ratios of $I_{(100)}/I_{(111)}$ for sample RD1 ($I_{(100)}/I_{(111)} = 0.89$) compared with the sample RD3 ($I_{(100)}/I_{(111)} = 1.02$) mainly resulted from the different etching efficiency of hydrogen ion on the non-(100)-oriented grains and the (100) grains. It is known that the etching efficiency of hydrogen ion on the non-(100)-oriented grains is more significant than that on the (100) grains. As a result, the (100) faces will survive due to the local chemical transport reaction while the non-(100) grains will be etched off [20–22]. Hence, sample RD1 has lower [100]-oriented intensity than sample RD3 although they were prepared with same methane concentration (0.34%). These results are consistent with the SEM observations of the surface morphologies of the investigated five samples, indicating that the methane concentration has great influence on the orientation of the films

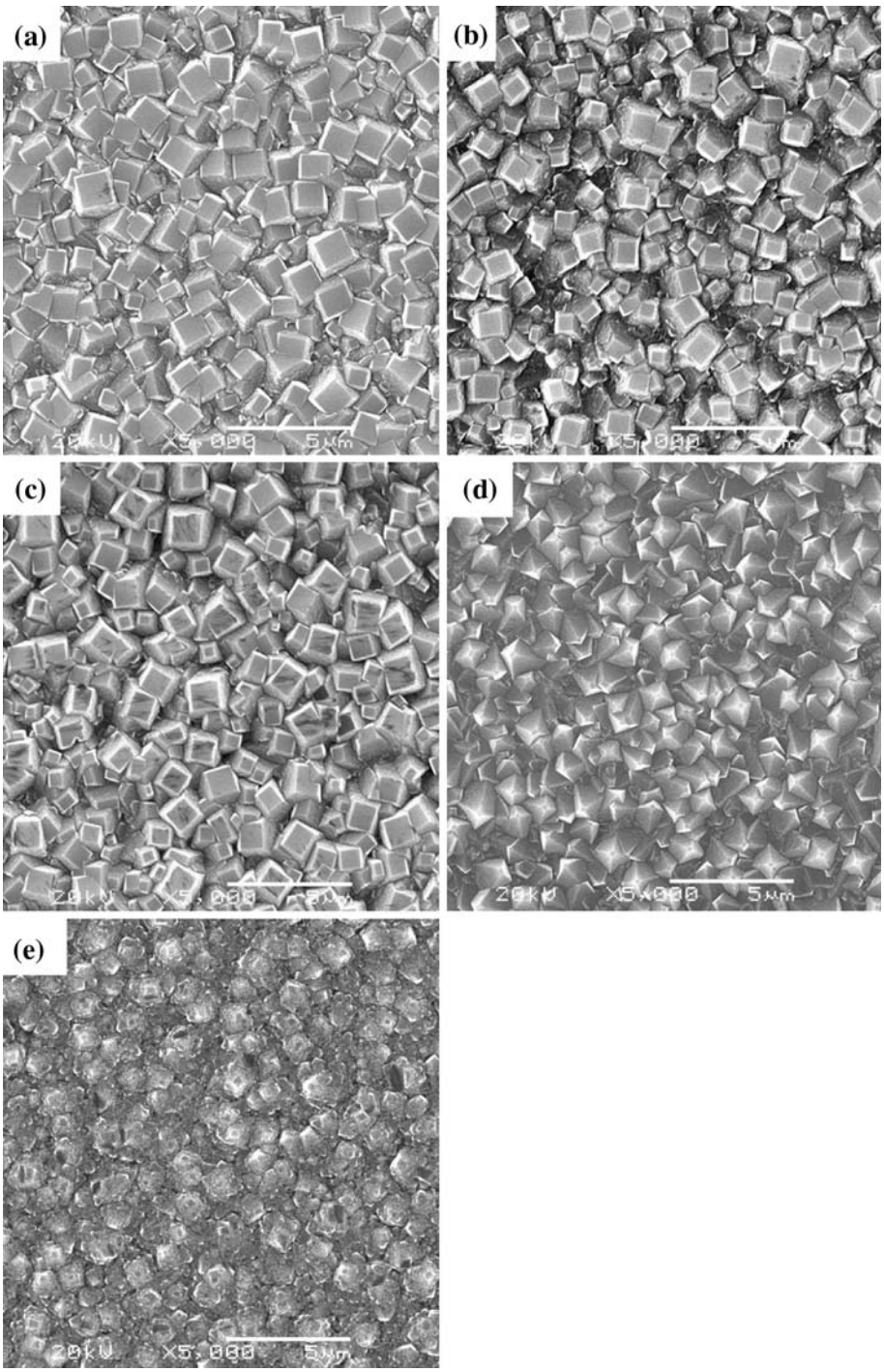

Fig. 2 SEM images of the diamond films prepared with the different methane concentrations: **a** [RD3] 0.34%; **b** [RD4] 0.43%; **c** [RD5] 0.51%; **d** [RD6] 0.60%; **e** [RD1] 0.34%

[23–25]. In addition, the resistivities of RD4, RD5, and RD6 from dark current measurements were 4.5×10^{14}, 3.2×10^{14}, and 1.2×10^{14} Ω cm, respectively.

Photocurrents at different X-ray fluxes for radiation dosimeters based on [100]-oriented diamond films with different intensity ratios using cyclic deposition technique are reported in Fig. 1. It can be seen that the responsive sensitivity is enhanced with the increase in the intensity ratio of $I_{(100)}/I_{(111)}$. This may be due to the lower concentrations of defects and the higher carrier drift length of the [100]-orientation films [26–29] with the increase in the preferential orientation intensity, thereby behaving better electrical performances to have higher photocurrent and sensitivity. Hence, increasing the intensity of preferential orientation of the diamond thin films may be beneficial for the improvement in the performance of the photoelectric response to X-ray. In addition, the worsening in the detection performance of RD4 and RD5 in comparison with RD3 may be

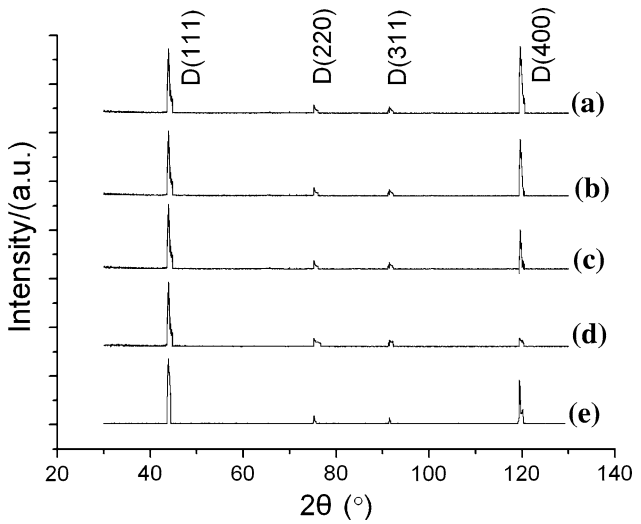

Fig. 3 XRD patterns of the diamond films prepared with the different methane concentrations: (*a*) [RD3] 0.34%; (*b*) [RD4] 0.43%; (*c*) [RD5] 0.51%; (*d*) [RD6] 0.60%; (*e*) [RD1] 0.34%

related to the enhanced defect density occurring at higher methane concentration [29].

Photocurrents of the radiation dosimeters RD5 and RD6 under the steady-state X-ray irradiation are also shown in Fig. 1. It can be observed that RD5 has higher sensitivity than RD6. From the obtained resistivities, it can be seen that RD5 and RD6 are all at about 10^{14} order of magnitude, the difference of the X-ray response sensitivity is mainly resulted from the different orientations of the diamond thin films. The [100]-oriented film has lower concentrations of defects, higher charge collection efficiency, and higher carrier drift length [26–29] than the [111]-oriented film, which leads to the higher sensitivity for RD5 in comparison with RD6.

Effect of in situ oxygen plasma post-treatment

Either a surface layer of graphite and/or of hydrogenated diamond, which behaves as a p-type diamond layer on the as-grown sample, are believed to be responsible for the measured low resistivity values [30]. On the as-grown samples, high leakage currents generate high noise. Such effects may preclude the use of as-grown diamond films for the radiation dosimeter fabrication. In order to minimize surface leakage currents, in situ oxygen plasma post-treatment was employed in our study. In XPS spectra, surface carbon combined states of the as-grown diamond thin film were assigned according to [31–33]: binding energy 283, 285, 287, and 289 eV were corresponding to C1 s deconvoluted component of C–H bond, graphite C, diamond C, and C–O bond, respectively. Figure 4 and Table 2 are the XPS spectra and the relative content of surface carbon combined states of the as-grown diamond thin film and the in situ oxygen plasma post-treated diamond film, respectively. It can be seen that the surface of the as-grown film RD7 has much more content of graphite C and C–H bond than that of the in situ oxygen plasma post-treated diamond film. There is almost no graphite C and C–H bond in the surface of the film treated by the in situ oxygen plasma treatment, which leads to the increase in the resistivity up to several orders of magnitude. The resistivity of the RD7 from dark current measurements was 5.9×10^{11} Ω cm, the decrease in the resistivity up to about three orders of magnitude compared with the resistivity of the in situ oxygen plasma post-treated diamond thin film, indicating that the in situ oxygen plasma post-treatment is a more effective means to improve the film surface purity due to the effective reduction of the graphite and C–H bond content on the surface of the film (as shown in Table 2).

Table 2 Relative content of surface carbon (C) combined states of the in situ oxygen plasma post-treated diamond film (RD3) and the as-grown diamond film (RD7)

Sample	Diamond (%)	Graphite (%)	C–H bond (%)	C–O bond (%)
RD3	93.5	0	0	6.5
RD7	71.9	8.9	10.9	8.1

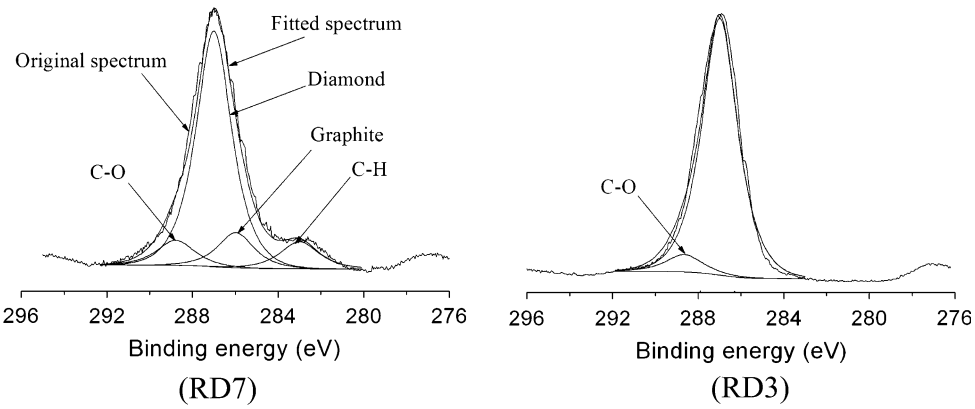

Fig. 4 XPS spectra of the in situ oxygen plasma post-treated diamond thin film (RD3) and the as-grown diamond thin film (RD7)

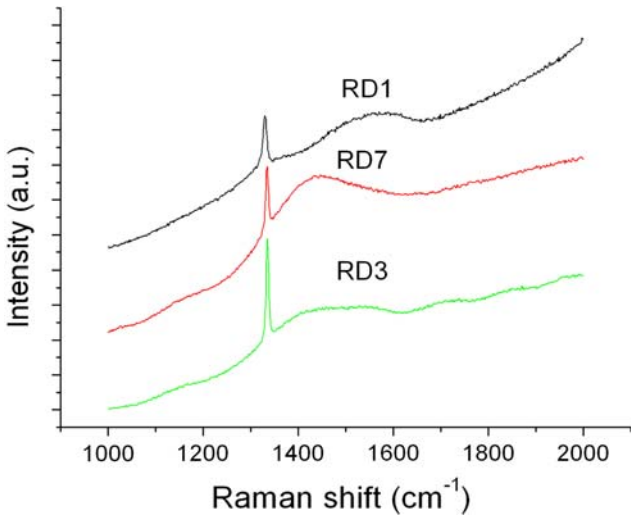

Fig. 5 Raman spectra of the in situ oxygen plasma post-treated diamond thin films (RD3), (RD1), and the as-grown diamond thin film (RD7)

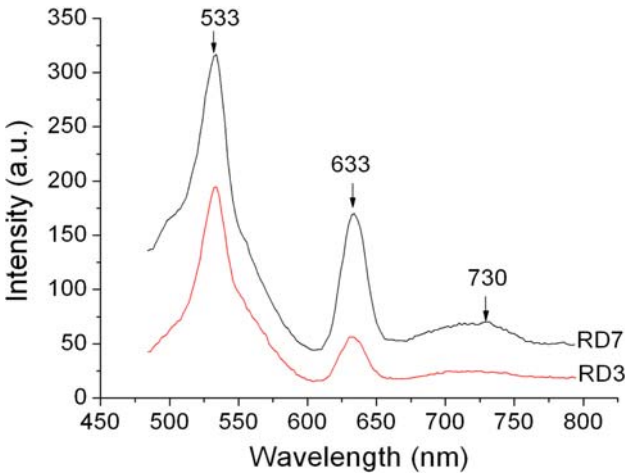

Fig. 6 PL spectra of the in situ oxygen plasma post-treated diamond thin film (RD3), the as-grown diamond thin film (RD7)

Raman spectroscopy is widely used as a tool for the evaluation of the phase purity and perfection of diamond films grown by CVD [34, 35]. Figure 5 shows the Raman spectra of MWPCVD diamond before (RD7) and after in situ oxygen plasma post-treatment process (RD3 and RD1). The untreated sample (RD7) showed a sharp diamond peak at 1332 cm^{-1} [35–37] along with weak broad peak at around 1500 cm^{-1}, indicating the presence of sp^2-bonded carbon in the form of amorphous carbon [38, 39]. However, the in situ oxygen plasma post-treated sample (RD3) showed the sharp diamond peak at 1332 cm^{-1} with only a weak feature of sp^2-bonded carbon phases, suggesting the improvement in the film quality. From the above SEM images and Raman analysis, it is evident that the cyclic deposition produces more well-faceted morphologies and the high-quality diamond film. These results are consistent with the results of XPS analysis. In addition, compared with the sample RD3, the Raman spectrum of sample RD1 showed that the broad peak in the range from 1400 to 1600 cm^{-1} clearly increases, characteristic of non-diamond carbon [19], indicating the deterioration of quality of diamond films prepared by nucleation-growth deposition technique. The PL spectra of the in situ oxygen plasma post-treated and untreated diamond samples are displayed in Fig. 6. The untreated sample (RD7) shows three PL bands centered at 533 nm (2.33 eV), 633 nm (1.96 eV), and 730 nm (1.68 eV). In contrast, the in situ oxygen plasma post-treated sample (RD3) shows only two weak PL bands centered at 533 nm (2.33 eV) and 633 nm (1.96 eV). The band centered at 533 nm (2.33 eV) is attributed to the presence of the sp^2-bonded carbon phases [35, 40, 41]. The results indicate that the plasma post-treatment can effectively etch the sp^2-bonded carbon impurities in the diamond, consistent with the results of XPS and Raman characterization. The PL band centered at 1.68 eV is attributed to a silicon-vacancy defect complex (Si–V), which has also been observed by other research groups [35, 42–44]. From Fig. 6, the decrease in the intensity of the silicon-vacancy can also be observed, showing that plasma post-treatment can also passivate the silicon-vacancy defect. In addition, the PL band centered at 1.96 eV is very close to the 1.945 eV attributed to the negative nitrogen-vacancy center [45]. Hence, it may be reasonable that the band centered at 1.96 eV is related to the nitrogen-vacancy defect. The decrease in the peak intensity at 633 nm suggests that in situ oxygen plasma post-treatment can also passivate the nitrogen-vacancy defect. PL spectra show the improvement in the film purity of plasma-treated diamond compared with the untreated diamond. From Fig. 1, it can be observed that the radiation dosimeter based on the in situ oxygen plasma post-treated diamond film (RD3) has higher sensitivity than that based on the as-grown diamond film (RD7), an increase by a factor of about 2, suggesting that the in situ oxygen plasma post-treatment can improve the sensitivity of the CVD diamond-based device. Moreover, our previous research shows that the sensitivity of the device based on sample RD3 (1.45×10^{-4}) is at the same order of magnitude as that of Si diode dosimeter (1.27×10^{-4}) [46], suggesting that it has the potential to be used in radiation dosimetry.

Time-dependent response to X-ray

Figure 7 shows the time-dependent photocurrents of the device, recorded every 2 min to the total time of 28 min, at the X-ray flux of 6.0×10^4 and 1.0×10^5 a.u., respectively. It can be seen that the signal increases rapidly in the first about 10 min, and then slowly achieving a stable value

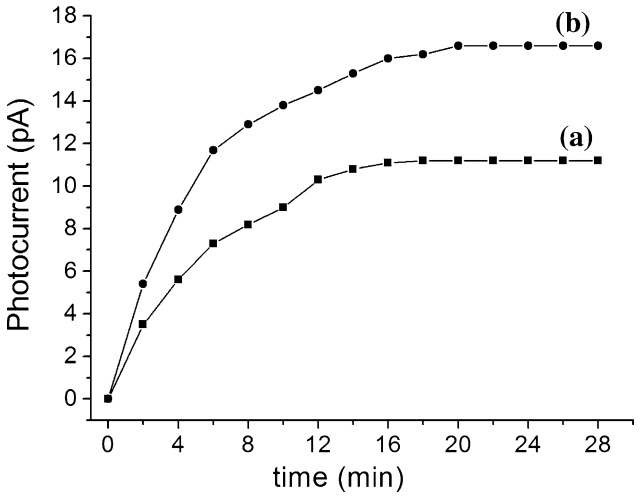

Fig. 7 Time-dependent response of the radiation dosimeter based on RD3 at different X-ray flux irradiations: (*a*) 6.0×10^4 a.u.; (*b*) 1.0×10^5 a.u.

after a period of about 16 min. The extended period to reach signal saturation is attributed to the filling of trapping states in the forbidden gap, and this phenomenon in the X-ray response has also been observed in other studies of CVD diamond radiation detectors [6, 7, 47]. Figure 7 shows also that the time to reach signal saturation for the studied sample is almost the same at the different X-ray fluxes, which suggests that the extended period to reach signal saturation for the device is mainly related to some deep-level defects and impurities within the diamond thin films. Deep levels in the diamond thin films can trap some of the carriers released by the irradiation, and the current signal achieves a stable value when these defects are almost filled.

Conclusions

The cyclic deposition process and the in situ oxygen plasma post-treatment increase the sensitivity of the device based on the diamond thin film. The increase in the methane concentration in the deposition gas mixture will worsen the irradiation response of the devices mainly resulted from the change of the orientation and purity of the films. XPS, PL, and Raman measurements suggest that the in situ oxygen plasma post-treatment can effectively etch non-diamond phases and passivate the silicon-vacancy and nitrogen-vacancy defects, resulting in an increase in the response sensitivity of the CVD diamond-based device by a factor of about 2. The X-ray response of the device also shows that the photocurrent signals achieve stable after 16 min due to the priming effect mainly resulted from some deep-level defects and impurities within the diamond thin films. However, more research is required to understand and remove it to improve the properties of the device promisingly used as an alternative in radiation dosimetry.

Acknowledgements This study was supported by the National Natural Science Foundation of China (No. 10275046). The authors would like to thank Mr. Jin Zhang of Southwest Petroleum University and Dr. Bing Wang of the Southwest University of Science And Technology for their kind help and instructive discussions.

References

1. Bruzzi M, Bucciolini M, Casati M, DeAngelis C, Lagomarsino S, Løvik I, Onori S, Sciortino S (2004) Nucl Instrum Methods Phys Res A 518:421
2. Ascarelli P, Cappellia E, Trucchi DM, Conte G (2003) Diamond Relat Mater 12:691
3. Fidanzio A, Azario L, Venanzi C, Pinzari F, Piermattei A (2002) Nucl Instrum Methods Phys Res A 479:661
4. Bruzzi M, Bucciolini M, Nava F, Pini S, Russo S (2002) Nucl Instrum Methods Phys Res A 485:172
5. Bruzzi M, Bucciolini M, Cirrone GAP, Cuttone G, Mazzocchi S, Pirollo S, Sciortino S (2000) Nucl Instrum Methods Phys Res A 454:142
6. Buttar CM, Conway J, Meyfarth R, Scarsbrook G, Selin PJ, Whitehead A (1997) Nucl Instrum Methods Phys Res A 392:281
7. Buttar CM, Airey R, Conway J, Hill G, Ramkumar S, Scarsbrook G, Sussmann RS, Walker S, Whitehead A (2000) Diamond Relat Mater 9:965
8. Jung M, Merer Ph, Morel J, Teissier C, Siffert P (2003) Nucl Instrum Methods Phys Res A 511:417
9. Ramkumar S, Buttar CM, Conway J, Whitehead AJ, Sussmann RS, Hill G, Walker S (2001) Nucl Instrum Methods Phys Res A 460:401
10. Assiamah M, Nam TL, Keddy KJ (2007) Appl Radiat Isot 65:545
11. Pini S, Bruzzi M, Bucciolini M, Borchi E, Lagomarsino S, Menichelli D, Miglio S, Nava F, Sciortino S (2003) Nucl Instrum Methods Phys Res A 514:135
12. Marinelli M, Milani E, Paoletti A, Tucciarone A, Rinati GV, Angelone M, Pillon M (2001) Diamond Relat Mater 10:645
13. Balducci A, Marinelli M, Milani E, Morgada ME, Pucella G, Rodriguez G, Tucciarone A, Verona-Rinati G, Angelone M, Pillon M (2005) Appl Phys Lett 86:022108
14. McKeag RD, Jackman RB (1998) Diamond Relat Mater 7:513
15. Barberini L, Cadeddu S, Caria M (2001) Nucl Instrum Methods Phys Res A 460:127
16. Marczewska B, Nowak T, Olko P, Nesladek M, Waligórski MPR (2001) Physica B 308–310:1213
17. Whitehead AJ, Aiery R, Buttar CM, Conway J, Hill G, Ramkumar S, Scarsbrook GA, Sussmann RS, Walker S (2001) Nucl Instrum Methods Phys Res A 460:20
18. Liao XM, Ran JG, Gou L, Zhang J, Su BH, Lin JL (2007) Key Eng Mater 336–338(II):1718
19. Spear KE (1989) J Am Ceram Soc 72:171
20. Su QF, Liu JM, Wang LJ, Shi WM, Xia YB (2006) Scr Mater 54:1871
21. Jiang X, Rickers C (2006) Appl Phys Lett 75:3935
22. Jiang X, Zhang WJ, Klages CP (1998) Phys Rev B 58:7064
23. Kim YK, Lee KY, Lee JY (1996) Thin Solid Films 272:64
24. Marinelli M, Milani E, Pace E, Paoletti A, Santoro M, Sciortino S, Tucciarone A, Verona-Rinati G (1998) Diamond Relat Mater 7:1039

25. Chen GC, Li B, Lan H, Dai FW, Zhou ZY, Askari J, Song JH, Hei LF, Li CM, Tang WZ, Lu FX (2007) Diamond Relat Mater 16:477
26. Jany C, Foulon F, Bergonzo P, Brambilla A, Silva F, Gicqel A, Pochet T (1996) Diamond Relat Mater 5:741
27. Jany C, Foulon F, Bergonzo P, Brambilla A, Gicqel A, Pochet T (1996) Nucl Instrum Methods Phys Res A 380:107
28. Xia YB, Sekiguchi T, Zhang WJ, Jiang X, Ju JH, Wang LJ, Yao T (2000) Diamond Relat Mater 9:1636
29. Donato MG, Faggio G, Marinelli M, Messina G, Milani E, Paoletti A, Santangelo S, Tucciarone A, Rinati GV (2001) Diamond Relat Mater 10:1788
30. Jany C, Foulon F, Bergonzo P, Marshall RD (1998) Diamond Relat Mater 7:951
31. Wang B, Ran JG, Gou L, Ji JG (2003) J Sichuan Univ (Eng Sci Ed) 35:58 (in Chinese)
32. Humbert B, Hellala N, Ehrhardt JJ, Barrat S, Bauer-grosse E (2008) Appl Surf Sci 254:6400
33. Fan Y, Fitzgerald AG, John P, Triope CE, Wilson JIB (2002) Surf Interface Anal 34:703
34. Knight DS, White WB (1989) J Mater Res 4:385
35. Wang SG, Sellin PJ, Zahng Q, Lohstroh A, Ozsan ME, Tian JZ (2005) Diamond Relat Mater 14:541
36. Solin SA, Ramdas AK (1970) Phys Rev B 1:1687
37. Kobashi K, Nishimura K, Kawate Y, Horiuchi T (1988) Phys Rev B 38:4067
38. Matsumoto S, Sato Y, Tsutsumi M, Setaka N (1982) J Mater Sci 17:3106. doi:10.1007/BF01203472
39. Sato T, Furuno S, Iguchi S, Hanabusa M (1988) Appl Phys A 45:355
40. Nesladek M, Stals LM, Stesmans A (1996) Appl Phys Lett 72:3306
41. Iakoubovskii K, Adriaenssens GJ (2000) Diamond Relat Mater 9:1017
42. Mckeag RD, Marshall RD, Baral B, Chan SSM, Jackman RB (1997) Diamond Relat Mater 6:361
43. Bergman L, Stoner BR, Turner JT, Glass KF, Nemanich RJ (1993) J Appl Phys 73:3951
44. Ruan J, Choyke WJ, Partlow WD (1991) Appl Phys Lett 58:295
45. Iakoubovskii K, Adriaenssens GJ, Nesladek M (2000) J Phys Condens Matter 12:189
46. Liao XM (2006) PhD thesis, Sichuan University, China (in Chinese)
47. Manfredotti C (2005) Diamond Relat Mater 14:531